

Gas-dynamic shock heating of post-flare loops due to retraction following localized, impulsive reconnection

D.W. Longcope,¹ S.E. Guidoni,¹ and M.G. Linton²

1. Department of Physics, Montana State University, Bozeman, Montana 59717

2. Naval Research Laboratory, Washington, D.C.

Draft: February 16, 2019

ABSTRACT

We present a novel model in which field lines shortening after localized, three-dimensional reconnection heat the plasma as they compress it. The shortening progresses away from the reconnection site at the Alfvén speed, releasing magnetic energy and generating parallel, compressive flows. These flows, which are highly supersonic when $\beta \ll 1$, collide in a pair of strong gas-dynamic shocks at which both the mass density and temperature are raised. Reconnecting field lines initially differing by more than 100° can produce a concentrated knot of plasma hotter than 20 MK at the loop’s apex, consistent with observations. In spite of these high temperatures, the shocks convert less than 10% of the liberated magnetic energy into heat — the rest remains as kinetic energy of bulk motion. These gas-dynamic shocks arise only when the reconnection is impulsive and localized in all three dimensions; they are distinct from the slow magnetosonic shocks of the Petschek steady-state reconnection model.

Subject headings: MHD — shock waves — Sun: flares

1. Introduction

Magnetic reconnection has long been proposed as a mechanism for heating coronal plasma. In one early model (Kopp & Pneuman 1976, see Fig. 1), reconnection occurs between open field lines separated by a vertical current sheet (red line) creating new closed field lines (post-flare loops, grey). Closing these field lines stops the solar wind upflow in a gas-dynamic shock (GDS) that Kopp & Pneuman (1976) estimated would raise the temperature by 80%. Cargill & Priest (1982) found the direct magnetic energy conversion by reconnection to be a far more effective source of heating in this same model. It could raise the temperature of post-flare loops by up to a factor of three to 6 MK. Even this higher value is, however, insufficient to explain the 15–20

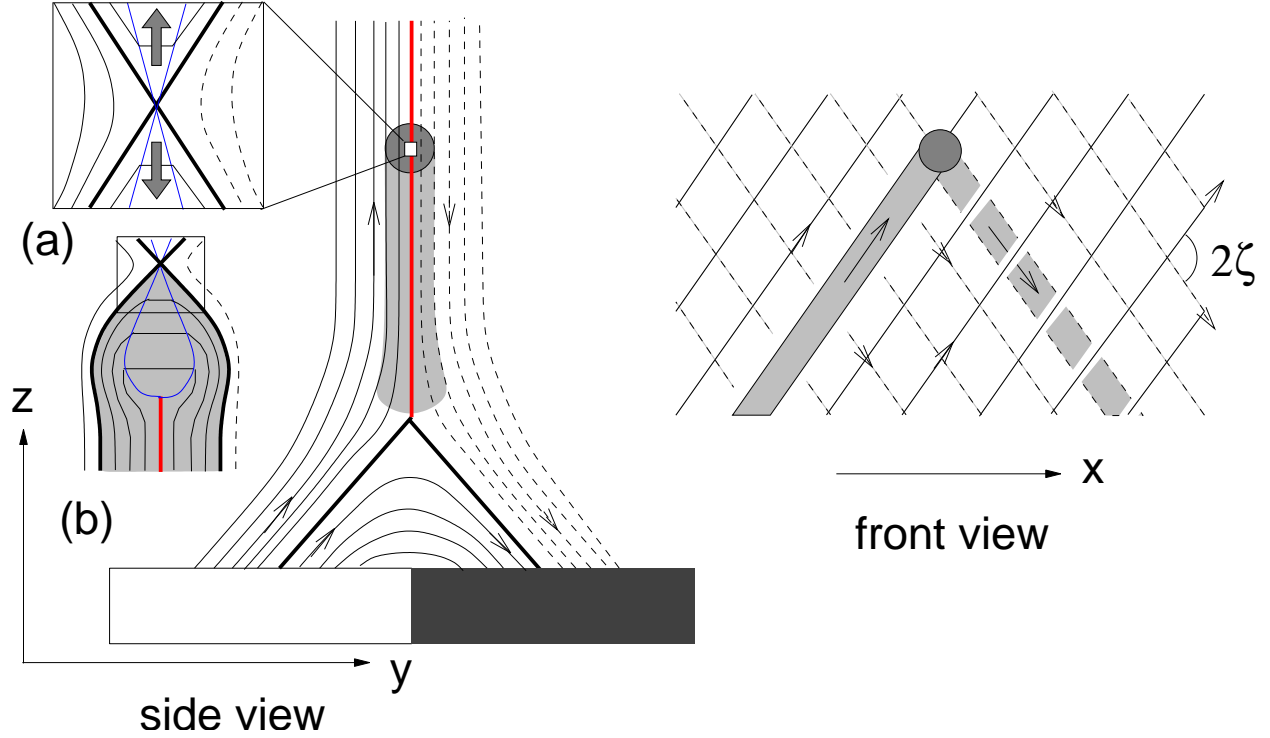


Fig. 1.— The classical Kopp-Pneuman model and its modifications. The side view (left) shows the basic two-dimensional geometry. Inset (a) on the upper left shows how steady Petschek reconnection is configured within the current sheet. Inset (b) on the lower left shows how a transient reconnection produces a finite layer of reconnected flux (grey). The front view (right) shows how the model becomes three-dimensional when the reconnection is localized in third dimension (x). Instead of a current layer the reconnection produces a Λ -shaped flux tube of closed field (grey); a completely detached, V-shaped flux tube (not shown) is created at the same time.

MK temperatures observed at apices of post-flare loops in Soft X-ray and Fe XXIV EUV emission (Warren et al. 1999).

Recent theoretical investigations have revealed that electric fields large enough for fast magnetic reconnection can be self-consistently produced by a wide range of small-scale mechanisms, provided only that they are localized within a segment of the current sheet (Birn et al. 2001; Biskamp & Schwarz 2001). All such processes generate reconnection flows resembling the model of Petschek (1964, see inset a) with slow magnetosonic shocks outside the non-ideal region (SMSs, blue lines) at which the magnetic field is deflected and weakened, thereby heating the plasma. When reconnection is localized in both space and time the SMSs close back together across a finite layer of horizontal field, as shown in inset (b) of Fig. 1 (Semenov et al. 1983; Biernat et al. 1987). This field forms the top of a “hairpin” comprising all the flux closed since the onset of reconnection.

As the hairpin flux sheet retracts its field lines become much shorter and releases substantial magnetic energy. This magnetic energy is converted almost entirely into kinetic energy rather than partly into heat as in Petschek’s steady state model (Semenov et al. 1998). In a strictly two-dimensional version of the model the mass of the shortened tube accumulates in the tip of the retracting hairpin. This “snowplowing” artifact is absent when reconnection is also localized in the third dimension (x) and there is a magnetic field component in that direction. With the horizontal field component (sometimes called a “guide field”) the current sheet separates field with angle 2ζ ($\tan \zeta = B_z/B_x$, see the “front view” of Fig. 1).

Flux reconnected within a patch and over a finite interval forms a Λ -shaped flux tube (grey) similar to magnetospheric *flux transfer events* (Russell & Elphic 1978; Lee et al. 1993; Otto 1995). The tube is distinguished from the surrounding field (the flux layers) by the distinct connectivity given it through reconnection. Different field line geometry, such as the bend, produce dynamics in the tube entirely different from those in the surrounding flux layers, with which it has little subsequent interaction.

Recently Linton & Longcope (2006) studied the relaxation of this post-reconnection flux tube using three-dimensional magnetohydrodynamic (MHD) simulation. They found that the perpendicular dynamics of the tube, as it moves between the flux layers, is well approximated by the equations for a thin magnetic flux tube (Spruit 1981), although with $\beta < 1$. They presented an analytic solution in which the post-reconnection tube shortens at the Alfvén speed, converting magnetic energy into kinetic energy. Linton & Longcope (2006) did not investigate the dynamics parallel to the tube or any associated thermal effects of shortening.

This letter demonstrates that flux tube shortening is a powerful, inevitable mechanism for heating post-flare loops, which has not been previously investigated. The magnetic forces respon-

sible for shortening, also drive compressive parallel flows at the Alfvén speed. At very low β , these are high-Mach number flows whose collision naturally generates very strong shocks. The shocks are distinct from the SMSs of Petschek reconnection and are driven by reconnection-initiated, perpendicular dynamics. This is in contrast to previous investigations of flux tube shocks wherein acoustic wave-steepening or pressure differences were considered as drivers (Herbold et al. 1985; Thomas & Montesinos 1991).

2. Post-reconnection flux tube dynamics

We begin by assuming that localized, transient, fast magnetic reconnection has occurred, by an unspecified physical mechanism, within an otherwise static current sheet. This will, as just discussed, leave a Λ -shaped flux tube, initially at rest. Due to its sharp bend it is out of equilibrium, and magnetic forces start it sliding downward between the magnetic layers separated by the current sheet.

The tube’s retraction, unhindered by the external flux layers, can be modeled using the *thin flux tube* equations of Spruit (1981) and subsequent authors (see, for example, the review by Fisher et al. 2000). While the high- β flux tubes in those previous investigations are confined by the pressure of the unmagnetized convection zone, our post-reconnection tube has very low β and is confined by the magnetic pressure of the flux layers outside the current sheet. The tube is an isolated entity distinguished from its surroundings by its connectivity (Linton & Longcope 2006; Linton et al. 2008). We assume sufficient collisionality to justify the use of MHD equations throughout.

The tube is assumed thin enough to be described only by its axis. Internal properties such as the magnetic field strength, B_i , pressure, p_i , and mass density ρ_i , are function only of axial position. The tube is also thin enough for fast magnetosonic waves to establish pressure balance across its diameter virtually instantaneously. This assumption constrains the internal properties to match those outside the flux tube: $B_i^2/8\pi + p_i = B_e^2/8\pi + p_e$, assumed to be uniform and constant.

We will also assume the plasma β to be always small. The main force on a section of tube is therefore the magnetic tension due to curvature of the axis $B_i^2(\partial\hat{\mathbf{t}}/\partial\ell)/4\pi$, where ℓ is arc-length and $\hat{\mathbf{t}} = \partial\mathbf{x}/\partial\ell$ is the unit tangent vector. Since it is ultimately the Lorentz force, it is natural that this force is strictly perpendicular to the axis ($\hat{\mathbf{t}} \cdot \partial\hat{\mathbf{t}}/\partial\ell = 0$).

The pressure gradient, $-\hat{\mathbf{t}} \partial p_i / \partial \ell$, is formally smaller, by a factor of β , than the magnetic tension. It is, however, the only force parallel to the axis, and is essential to arresting internal pile-up of mass. We therefore retain terms involving pressure to first order in β .

Velocity evolution is governed by a momentum equation with only these two forces. Conservation properties become apparent when arc-length is replaced with μ , the integrated mass per unit flux: $\partial\mu/\partial\ell = \rho_i/B_i$. The value of μ never changes for a given fluid element. The resulting momentum equation

$$\frac{d\mathbf{v}}{dt} = \frac{B_i}{4\pi\rho_i} \frac{\partial}{\partial\ell}(B_i\hat{\mathbf{t}}) = \frac{\partial}{\partial\mu} \left(\frac{B_i\hat{\mathbf{t}}}{4\pi} \right) , \quad (1)$$

includes the parallel pressure gradient after use of pressure balance, $B_i = B_e + 4\pi(p_e - p_i)/B_e$, valid to first order in β . The momentum per unit flux of any section of tube,

$$\mathbf{P} = \int \frac{\rho_i\mathbf{v}}{B_i} d\ell = \int \mathbf{v} d\mu , \quad (2)$$

changes only through forces (per unit flux) from the ends of the section, $B_i\hat{\mathbf{t}}/4\pi$, directed parallel to the axis.

3. Shock relations in thin flux tubes

Momentum conservation leads to a set of shock relations for thin flux tubes. Consider two straight sections with uniform properties (designated 1 and 2), separated by an abrupt change at coordinate μ_0 . The length-scale of this change is large compared to the tube radius but otherwise small enough that we hereafter call it a “discontinuity” and “corner”.¹ This feature moves through space at constant velocity \mathbf{u} while its Lagrangian coordinate changes at constant rate $\dot{\mu}_0$. We assume that the properties of the straight sections do not change as this happens. Fluid velocities on either side of the discontinuity differ from \mathbf{u} , but components perpendicular to the tangent vector match that of \mathbf{u} : $(\mathbf{v} - \mathbf{u}) \times \hat{\mathbf{t}} = 0$.

The component of relative velocity parallel to the tangent vector, $v_{\parallel} = \hat{\mathbf{t}} \cdot (\mathbf{v} - \mathbf{u})$, represents a flow across the discontinuity. The mass flux (per magnetic flux) through the discontinuity, $\dot{\mu}_0$, must equal the mass flux across points on either side of it, since the corner moves without changing. For positions μ_1 and μ_2 , separated by fixed distances from μ_0 this means

$$\dot{\mu}_2 = - \rho_i v_{\parallel} / B_i \Big|_2 = - \rho_i v_{\parallel} / B_i \Big|_1 = \dot{\mu}_1 = \dot{\mu}_0 . \quad (3)$$

¹Analysis of the discontinuity’s internal structure must be done outside the thin-tube approximation. Doing so will probably reveal its length-scale to be comparable to the tube’s radius. This is analogous to non-ideal effects resolving internal structure of a hydrodynamic shock at scales comparable to the mean free path (Grad 1951). Following that analogy, the thin flux tube equations provide external conservation laws leading to the shock relations.

The flux tube between μ_2 and μ_1 does not change so its momentum (per magnetic flux) is constant,

$$\dot{\mathbf{P}} = \llbracket \dot{\mu} \mathbf{v} \rrbracket + \llbracket B_i \hat{\mathbf{t}} / 4\pi \rrbracket = 0 \quad , \quad (4)$$

denoting $\llbracket f \rrbracket = f_2 - f_1$. Since $\mathbf{v} = \mathbf{u} + v_{\parallel} \hat{\mathbf{t}}$ away from the discontinuity momentum constancy may be written

$$\langle B_i / 4\pi - \rho_i v_{\parallel}^2 / B_i \rangle \llbracket \hat{\mathbf{t}} \rrbracket - \llbracket p_i / B_e + \rho_i v_{\parallel}^2 / B_i \rrbracket \langle \hat{\mathbf{t}} \rangle = 0 \quad , \quad (5)$$

where $\langle f \rangle = (f_2 + f_1)/2$.

The vectors $\llbracket \hat{\mathbf{t}} \rrbracket$ and $\langle \hat{\mathbf{t}} \rangle$ are orthogonal so eq. (5) represents two independent equations. As long as the bend is not a hairpin ($\langle \hat{\mathbf{t}} \rangle \neq 0$) the $\langle \hat{\mathbf{t}} \rangle$ component of momentum conservation, to lowest order in β , is equivalent to gas-dynamic momentum conservation: $\llbracket p_i + \rho_i v_{\parallel}^2 \rrbracket = 0$. To the same order in β , eq. (3) gives the gas-dynamic mass continuity equation: $\llbracket \rho_i v_{\parallel} \rrbracket = 0$. Provided there is no heat flow from the external field or across μ_1 or μ_2 , then the sum of kinetic and thermal energy within the tube section will also be conserved. This provides one additional, independent constraint on ρ_i , p_i and v_{\parallel} across the discontinuity. (Since B_i can be related directly to p_i it can be eliminated from energy conservation.)

The foregoing describes three relations between six quantities which do not include the magnetic field's strength or direction. The relations are the traditional gas-dynamic Rankine-Hugoniot conditions (Courant & Friedrichs 1948), but for flows inside a flux tube (Ferriz-Mas & Moreno-Insertis 1987). The other component of eq. (5), to lowest order in β ,

$$\langle 1 - (4\pi\rho_i/B_e^2)v_{\parallel}^2 \rangle \llbracket \hat{\mathbf{t}} \rrbracket^2 = 0 \quad . \quad (6)$$

constitutes one more relation, which does involve the field direction.

From values on one side the Rankine-Hugoniot relations may be satisfied in two different ways by values on the other (see for example Courant & Friedrichs 1948). They may be satisfied non-trivially by a unique set of *different* values, or they may be satisfied trivially by the *same* set of values (i.e. $\llbracket \rho_i \rrbracket = \llbracket v_{\parallel} \rrbracket = \llbracket p_i \rrbracket = 0$). In the non-trivial case, the three different quantities satisfy three independent constraints and cannot be forced, in general, to satisfy a fourth. The leading factor of eq. (6), however, constitutes a fourth independent constraint so it will not in general vanish; it is therefore necessary that $\llbracket \hat{\mathbf{t}} \rrbracket = 0$ (there is no bend). This means that a thin, low- β flux tube can support discontinuities in internal quantities only at a GDS within a straight section of tube.

If, on the other hand, there *is* a bend in the flux tube ($\llbracket \hat{\mathbf{t}} \rrbracket \neq 0$), the only way to satisfy eq. (6) is for the pre-factor to vanish. Since the non-trivial solution of all three Rankine-Hugoniot conditions would over-determine the system, they must be satisfied trivially, without discontinuity. In other words ρ_i , and v_{\parallel} are continuous at μ_0 and satisfy the relation $v_{\parallel} = B_e / \sqrt{4\pi\rho_i} = v_A$ the Alfvén

speed. This is similar to an intermediate shock (Priest & Forbes 2000), but includes the influence of fast magnetosonic waves assumed to be maintaining pressure balance across the tube.

4. Shocks in the retracting flux tube

The Λ -shaped bend in the post-reconnection flux tube shown in Fig. 1 will immediately decompose into four different shocks of the kinds described above. Two intermediate shocks (bends, B) propagate along the field lines, forming a straight horizontal section between them (see Fig. 2), as previously found by Linton & Longcope (2006). Two GDSs propagate away from the center, at $\pm v_s$, along the horizontal section. This symmetric arrangement divides the tube into sections labeled, 3, 2 and 1, outward from the center.

Section 1 consists of the flux tube at rest and in its initial state: $\mathbf{v}_1 = 0$, $\rho_1 = \rho_e$ and $p_1 = p_e$. The initial field lines are inclined at angle ζ , so $\hat{\mathbf{t}}_1 = \hat{\mathbf{x}} \cos \zeta - \hat{\mathbf{z}} \sin \zeta$, while $\hat{\mathbf{t}}_2 = \hat{\mathbf{x}}$ in the horizontal section. The bend propagates along the initial field at the Alfvén speed: $\mathbf{u} = v_{A,e} \hat{\mathbf{t}}_1$. The relative parallel flow is continuous across the bend $v_{\parallel,1} = v_{\parallel,2} = -v_{A,e}$. These facts can be combined into the post-bend fluid velocity

$$\mathbf{v}_2 = \mathbf{u} + v_{\parallel} \hat{\mathbf{t}}_2 = -2v_{A,e} \sin^2(\zeta/2) \hat{\mathbf{x}} - v_{A,e} \sin \zeta \hat{\mathbf{z}} , \quad (7)$$

directed along the bisector of the bend (the mean direction of the curvature force).

Internal quantities are continuous across the bends, so $\rho_2 = \rho_1 = \rho_e$ and $p_2 = p_1 = p_e$. From a reference frame moving downward at $-\hat{\mathbf{z}} v_{A,e} \sin \zeta$, sections 2 and 3 appear to form a classic shock tube, with inflow at

$$M_2 = \frac{|v_{x,2}|}{c_{s,e}} = \sqrt{\frac{8}{\gamma \beta_e}} \sin^2(\zeta/2) , \quad (8)$$

where $\gamma = 5/3$ is the ratio of specific heats. Since $\beta_e \ll 1$, this Alfvénic inflow can have extremely high Mach number when field lines of significantly different orientation reconnect.

This supersonic inflow is brought to rest, $v_{x,3} = 0$, by a GDS moving outward at v_s . This stopping shock, equivalent to a piston moving into stationary fluid at speed $|v_{x,2}|$, is a classic problem (see §69 from Courant & Friedrichs 1948, for example), for which the solution is

$$v_s/|v_{x,2}| = \sqrt{M_2^{-2} + (\gamma + 1)^2/16} - \frac{1}{4}(3 - \gamma) . \quad (9)$$

The density ratio, $\rho_3/\rho_2 = 1 + |v_{x,2}|/v_s$, following from mass conservation, approaches the well-known limit $\rho_3/\rho_e = (\gamma + 1)/(\gamma - 1) = 4$, at large Mach numbers.

The post-shock pressure and plasma β also follow from the shock relations

$$\beta_3 = \beta_e [1 + \gamma M_2^2 (1 + v_s/|v_{x,2}|)] . \quad (10)$$

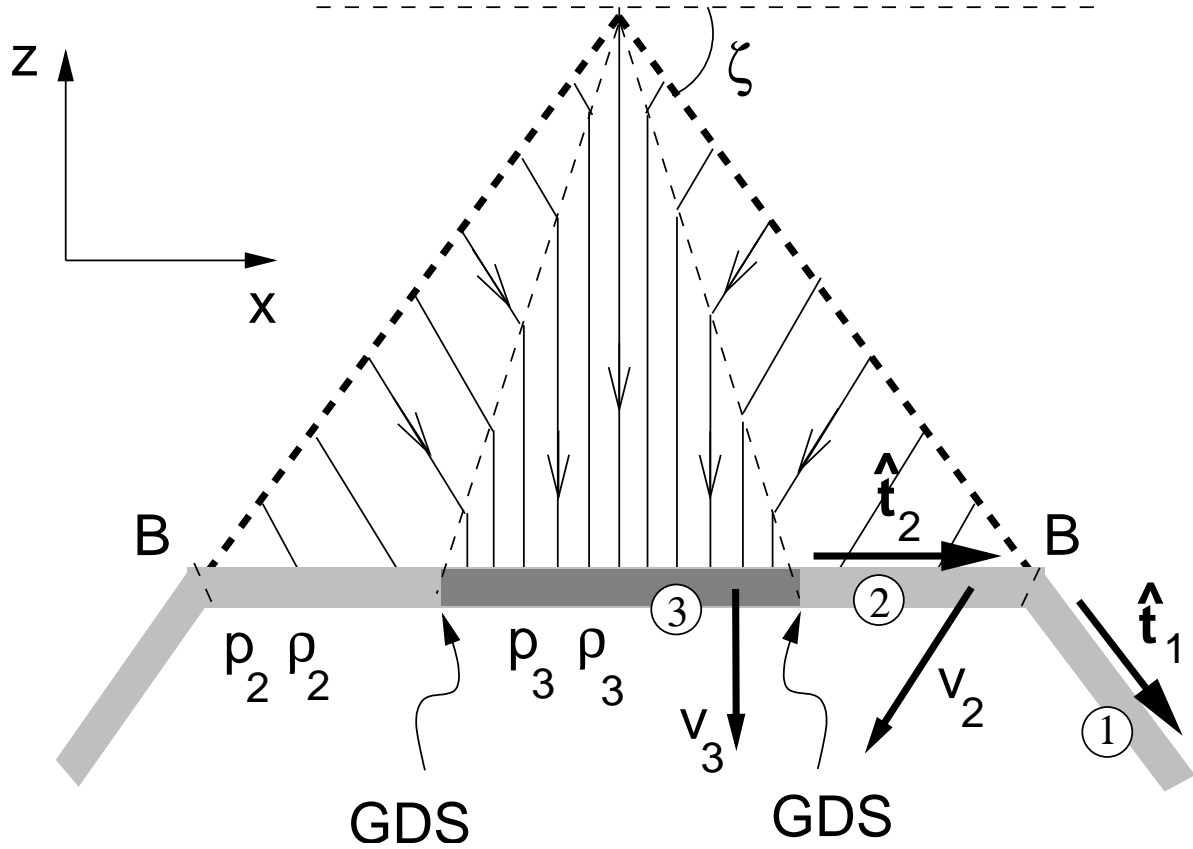


Fig. 2.— The flux tube retracting from the Λ -shaped initial condition shown in Fig. 1. This initial configuration is shown by thick dashed lines, while its current state is shown in grey. The past trajectory of the fluid, shown by solid lines, is initially focused inward. The gas-dynamic shocks (GDS) redirect the flow vertically; their past positions are shown by a thin dashed line. Circled numbers designate the states, 1, 2 and 3, separated by these shocks.

Even in the limit of vanishing pre-shock pressure ($\beta_e \ll 1$ and consequently $M_2 \gg 1$), the post-shock plasma can have significant pressure, $\beta_3 \simeq 4(\gamma + 1) \sin^4(\zeta/2)$. Our low- β assumption thereby imposes a limit on the reconnection angle; only for $\zeta < 67^\circ$ is $\beta_3 < 1$.

The post-shock temperature is then more conveniently expressed with respect to $T_e^A = (m_p/k_B)v_{A,e}^2/2$, than to the initial temperature. For example, 15 G field immersed in $n_e = 3 \times 10^8 \text{ cm}^{-3}$ plasma has a characteristic temperature $T_e^A = 2 \times 10^8 \text{ K}$. The plasma beta is $\beta_e = T_e/T_e^A$, so a 2 MK coronal plasma will have $\beta_e = 10^{-2}$. Figure 3a–b shows the post-shock temperature, $T_3 = T_e^A \beta_3 \rho_e / \rho_3$, over a range of β_e – ζ parameter space. For $\beta_e = 0.01$ and $\beta_3 = 1/3$ (the edge of the light grey area, $\zeta \simeq 50^\circ$) the post-shock plasma will be $T_3 = 0.1 T_e^A = 20 \text{ MK}$.

5. Energetics

By time t after the end of reconnection the two bends have passed over a total length $L = 2v_{A,e}t$. All of the mass in this tube is initially accelerated to a speed $|\mathbf{v}_2|$, giving it a kinetic energy (per cross sectional area)

$$\Delta W = \frac{1}{2} \rho_e |\mathbf{v}_2|^2 L = 2v_{A,e}^2 L \rho_e \sin^2(\zeta/2) . \quad (11)$$

The tube section has shortened by $\Delta L = 2L \sin^2(\zeta/2)$, thereby decreasing its internal magnetic energy (per area) by $\Delta W_m = B_e^2 \Delta L / 8\pi$, to lowest order in β_e . The background magnetic field fills the vacated volume doing work ΔW_m on the retracting tube, so the liberated energy in eq. (11), is twice ΔW_m .

The moving mass is deflected downward by the GDS, converting a portion of its kinetic energy into thermal energy. The kinetic energy (per area) converted to thermal energy, $\rho_3 v_{x,2}^2 v_s t$, constitutes a fraction

$$\frac{\Delta E_t}{\Delta W} = \frac{\rho_3 v_{x,2}^2 v_s}{\rho_e |\mathbf{v}_2|^2 v_{A,e}} = 2 \left(1 + \frac{v_s}{|v_{x,2}|} \right) \sin^4(\zeta/2) , \quad (12)$$

of the total (see Fig. 3c). Cases of vanishing initial pressure ($\beta_e \ll 1$) will have a fraction $(\gamma + 1) \sin^4(\zeta/2)$ of the released energy thermalized. Compression work done on larger initial pressure will raise this fraction slightly, but all cases with $\beta_3 < 1/3$ thermalize less than 10% of the released energy.

6. Summary

The foregoing illustrates, through a simplified analytic model, a process we believe must be common in the flaring corona. Localized reconnection does not directly dissipate magnetic energy, but rather initiates its release through subsequent shortening of field lines. This shortening propagates from the reconnection site at the Alfvén speed, converting energy from magnetic into kinetic form. The shortening flux tubes compress plasma within them, raising its temperature as they do so. Due to the supersonic (Alfvénic) flows this compression occurs at strong shocks, which raise the temperature far beyond that from adiabatic compression.

Both the GDS in our model and the SMS in Petschek’s model result, ultimately, from shortening or weakening of magnetic field lines. The two-dimensional Petschek model permits shortening only perpendicular to symmetry direction, accompanied by weakening. The shock is therefore a SMS whose normal is mostly perpendicular to the sheet. After three-dimensional patchy reconnection, on the other hand, field lines also shorten in the erstwhile symmetry direction which is the orientation of the shock normal ($\pm\hat{x}$). The GDSs are disconnected from the diffusion region, and are instead features of the ideal relaxation *following* reconnection. This new scenario requires two-step energy conversion, from magnetic to kinetic to thermal energy, in contrast to the SMSs which thermalize magnetic energy directly where they weaken the field.

This work was supported by NASA and the NSF.

REFERENCES

- Biernat, H. K., Heyn, M. F., & Semenov, V. S. 1987, JGR, 92, 3392
- Birn, J., et al. 2001, JGR, 106, 3715
- Biskamp, D., & Schwarz, E. 2001, Phys. Plasmas, 8, 4729
- Cargill, P. J., & Priest, E. R. 1982, Solar Phys., 76, 357
- Courant, R., & Friedrichs, K. O. 1948, Supersonic Flows and Shock Waves (New York: Interscience Publishers)
- Ferriz-Mas, A., & Moreno-Insertis, F. 1987, A&A, 179, 268
- Fisher, G. H., Fan, Y., Longcope, D. W., Linton, M. G., & Abbett, W. P. 2000, Phys. Plasmas, 7, 2173
- Grad, H. 1951, Comm. in Pure and App. Math., 5, 257

- Herbold, G., Ulmschneider, P., Spruit, H. C., & Rosnr, R. 1985, *A&A*, 145, 157
- Kopp, R. A., & Pneuman, G. W. 1976, *Solar Phys.*, 50, 85
- Lee, L. C., Ma, Z. W., Fu, Z. F., & Otto, A. 1993, *JGR*, 98, 3943
- Linton, M. G., DeVore, C. R., & Longcope, D. W. 2008, *Earth, Planets and Space* (in press)
- Linton, M. G., & Longcope, D. W. 2006, *ApJ*, 642, 1177
- Otto, A. 1995, *JGR*, 100, 11863
- Petschek, H. E. 1964, in *AAS-NASA Symposium on the Physics of Solar Flares*, ed. W. N. Hess (Washington, DC: NASA), 425
- Priest, E. R., & Forbes, T. G. 2000, *Magnetic Reconnection. MHD theory and applications* (Cambridge University Press)
- Russell, C. T., & Elphic, R. C. 1978, *Space Sci. Rev.*, 22, 681
- Semenov, V. S., Heyn, M. F., & Kubyshkin, I. V. 1983, *Sov. Astron.*, 27, 600
- Semenov, V. S., Volkonskaya, N. N., & Biernat, H. K. 1998, *Phys. Plasmas*, 5, 3242
- Spruit, H. C. 1981, *A&A*, 98, 155
- Thomas, J. H., & Montesinos, B. 1991, *ApJ*, 375, 404
- Warren, H. P., Bookbinder, J. A., Forbes, T. G., Golub, L., Hudson, H. S., Reeves, K., & Warshall, A. 1999, *ApJ*, 527, L121

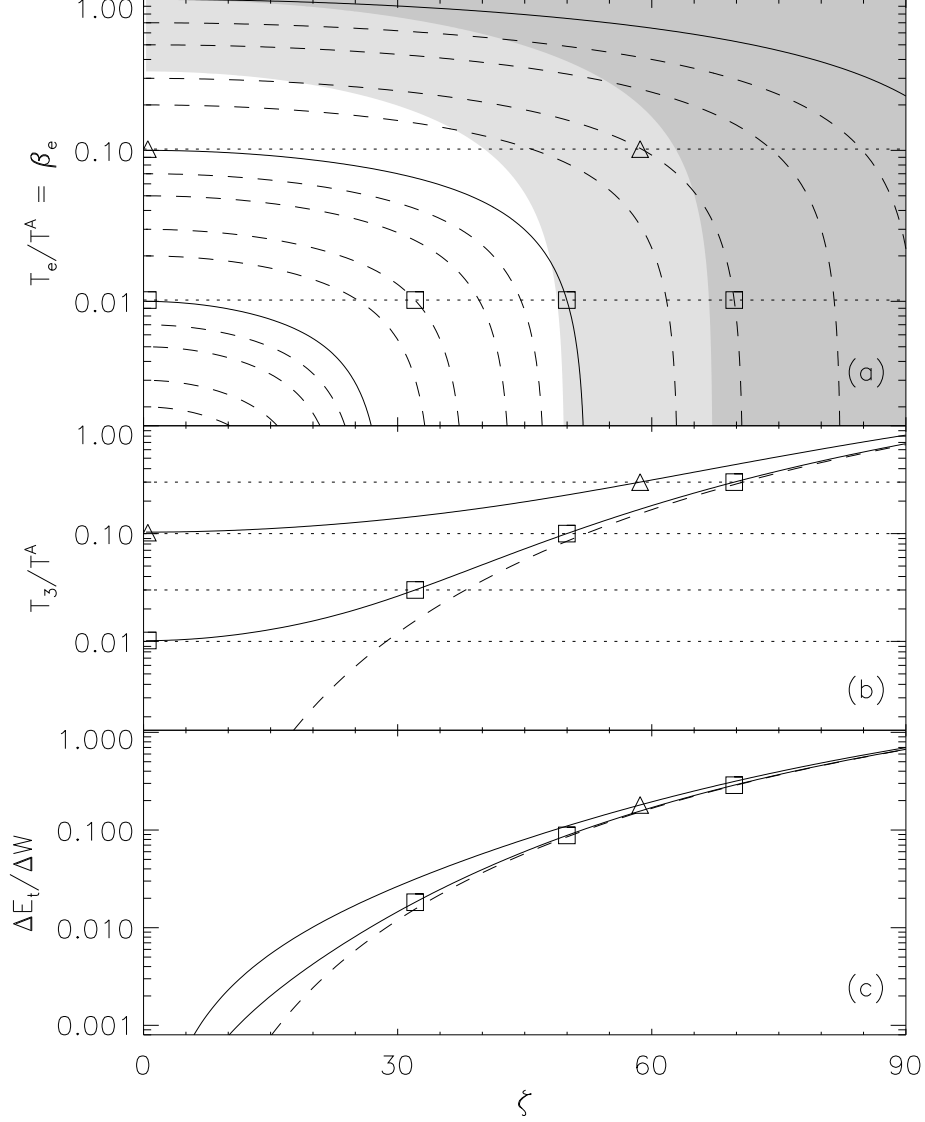


Fig. 3.— The post-shock temperature and thermal energy across the ζ – β_e parameter space. The top panel (a) shows contours of T_3 whose levels can be determined from intersection with the left axis ($\zeta = 0$) since $T_3 = T_e$ there. Solid contours show $T_3 = 0.01, 0.1$ and 1 (all in units of T_e^A). Light and dark grey regions show $0.333 < \beta_3 < 1$ and $\beta_3 > 1$ respectively. The middle panel (b) shows T_3 versus ζ for the values $T_e = \beta_e = 0.01$ (squares) and 0.1 (triangles). The bottom dashed curve is limit for the case $\beta_e = 0$. The bottom panel (c) shows, for the same values of $T_e = \beta_e$, the fraction of released energy thermalized by the GDS. Symbols show the same point in each panel.